Global and Planetary Change 168 (2018) 54–66

Contents lists available at ScienceDirect

Global and Planetary Change

journal homepage: www.elsevier.com/locate/gloplacha

Research article

Paleo-ENSO revisited: Ecuadorian Lake Pallcacocha does not reveal a conclusive El Niño signal

Tobias Schneider[a,b], Henrietta Hampel[c,d], Pablo V. Mosquera[e,f], Wojciech Tylmann[g], Martin Grosjean[a,b,*]

[a] Oeschger Centre for Climate Change Research, University of Bern, 3012 Bern, Switzerland
[b] Institute of Geography, University of Bern, Erlachstrasse 9a, 3012 Bern, Switzerland
[c] Facultad de Ciencias Químicas, Universidad de Cuenca, Cuenca, Ecuador
[d] Laboratorio de Ecología Acuática, Departamento de Recursos Hídricos y Ciencias Ambientales, Universidad de Cuenca, Cuenca, Ecuador
[e] Subgerencia de Gestión Ambiental, Empresa Pública Municipal de Telecomunicaciones, Agua potable, Alcantarillado y Saneamiento (ETAPA EP), Cuenca, Ecuador
[f] Departament de Biologia Evolutiva, Ecologia i Ciències Ambientals, Universitat de Barcelona, Barcelona, Spain
[g] Faculty of Oceanography and Geography, University of Gdansk, Bazynskiego 4, 80309 Gdansk, Poland

ARTICLE INFO

Keywords:
Holocene
Andes
Paleolimnology
Limnogeology
ENSO
Climate change

ABSTRACT

Information about decadal to millennial variability of El Niño Southern Oscillation (ENSO) is fundamental for the assessment of ENSO responses to natural and anthropogenic forcings. Despite a growing number of ENSO reconstructions, the overall picture of Holocene ENSO variability is inconsistent. Here, we revisit the iconic Holocene ENSO sediment record of Lake Pallcacocha, Ecuador (Rodbell et al., 1999). We asked: (i) How coherent are the records of clastic layers (flood layers) in the sediments of Lake Pallcacocha and adjacent Lake Fondococha? (ii) What are the synoptic-scale atmospheric conditions that lead to intense precipitation and, potentially, to alluvial activity promoting the deposition of clastic layers in these lakes? (iii) Is intense precipitation in this area associated with El Niño, or not?

We analyzed clastic layers in Late-Holocene sediments from multiple cores in Lakes Pallcacocha and Fondococha from Cajas National Park, southern Ecuadorian Andes. Additionally, we investigated precipitation data from 13 nearby meteorological stations to test if intense precipitation (percentiles $P_{0.95}$, $P_{0.99}$, $P_{0.995}$) is predominantly related to El Niño conditions or not (based on 15 different ENSO indices). Our results show that the absolute flood frequencies (clastic layers per 100 years) differ substantially from lake to lake. This indicates that the frequency of clastic layers reflects different sensitivities (thresholds of precipitation) of the catchments to alluvial activity. ^{210}Pb ages suggest that neither the 1982/83 nor the 1997/98 very strong El Niños produced clastic layers comparable to those found in the late Holocene. Daily precipitation records from meteorological stations close to Lake Pallcacocha including a high-altitude station from the western slope of the Andes did not show unusually high precipitation during the super El Niño 2015/16. We further find that intense precipitation in this area occurs at roughly equal probability under El Niño, La Niña and neutral conditions. Although the spectral properties of the late Holocene clastic layers in Lake Pallcacocha fall into the typical ENSO frequency band, we do not find evidence in the recent sediments and the meteorological data that would support a diagnostic link between alluvial activity in Lake Pallcacocha and strong El Niño events. Our data do not support the idea that the (late) Holocene flood record of Lake Pallcacocha is a conclusive paleo-El Niño record.

1. Introduction

The El Niño Southern Oscillation (ENSO) is the dominant source of inter-annual climate variability in the tropics (Wang et al., 2017 and references therein) and has significant impacts on ecosystems and societies (Stenseth et al., 2002). Despite remarkable advances in the understanding of ENSO dynamics and variations in space and time, little is known about the partitioning of its forcings and how these govern low frequency (decadal, centennial, millennial) ENSO variability (Ault et al., 2013; Cobb et al., 2013). However, this information is fundamental to help reduce uncertainty of ENSO behavior under global warming (Cai et al., 2015).

ENSO reconstructions from paleoclimate archives help extend empirical evidence of ENSO beyond the instrumental period. Based on

* Corresponding author at: Institute of Geography, University of Bern, Erlachstasse 9a T3, 3012 Bern, Switzerland.
E-mail addresses: tobias.schneider@giub.unibe.ch (T. Schneider), wojciech.tylmann@ug.edu.pl (W. Tylmann), martin.grosjean@oeschger.unibe.ch (M. Grosjean).

https://doi.org/10.1016/j.gloplacha.2018.06.004
Received 9 February 2018; Received in revised form 5 June 2018; Accepted 7 June 2018
Available online 09 June 2018
0921-8181/

comprehensive networks of annually resolved proxy data from the tropical Pacific (center of action) and adjacent areas with strong teleconnections, several centennial- to millennial-long ENSO reconstructions were proposed (mainly Nino 3.4 SSTs or SOI; (Braganza et al., 2009; Emile-Geay et al., 2013; Mann et al., 2008; Mcgregor et al., 2010; Wilson et al., 2010; Yan et al., 2011). Despite careful data selection, however, these reconstructions yield conflicting rather than consistent results (Ault et al., 2013; Baker and Fritz, 2015; Braconnot et al., 2012; Wilson et al., 2010; Zhang et al., 2014). The breakdown of inter-reconstruction coherency has been attributed to a lack of data, dating errors, differences in data treatment, changing teleconnections, distinct types ('flavors') of ENSO (Ault et al., 2013; Emile-Geay et al., 2013; Wilson et al., 2010) or to a non-linear behavior of the proxy-climate relationship (Emile-Geay and Tingley, 2016). Braconnot et al. (2012) emphasized the need to reinvestigate proxy records in order to better understand their relation to climate variability. Remarkable inconsistencies also exist in documentary-based ENSO reconstructions (Garcia-Herrera et al., 2008).

Compared with reconstructions spanning the last millennium, Holocene-long multi-site multi-proxy ENSO reconstructions (Donders et al., 2008) and even single-site reconstructions (e.g. Chen et al., 2016; Cobb et al., 2013; Conroy et al., 2008; Zhang et al., 2014 and references therein) are rare. Among the single-proxy single-site records, the ENSO reconstruction from Lake Pallcacocha (SW Ecuadorian Andes, 4050 m a.s.l.) acquired iconic status. In the sediments of this small, high-elevation Andean lake in Cajas National Park, Rodbell et al. (1999) uncovered numerous thin clastic laminae and interpreted these as deposits of alluvial activity after intense rainfall. In the absence of local meteorological data, the authors compared Pallcacocha to the Ecuadorian Pacific coast where, indeed, intense rainfall is typically related to El Niño (warm ENSO) phases (Vicente-Serrano et al., 2017). As a consequence, Rodbell et al. (1999) and, later, Moy et al. (2002), used the clastic laminae in Lake Pallcacocha to infer that El Niño events were less frequent in the early Holocene but became more frequent around 7000 yr BP, reaching modern values around 5000 yr BP. After culminating around 1200 yr BP, El Niño frequency was thought to decline to modern values. The Pallcacocha El Niño record showed prominent variability in the multi-centennial to millennial frequency domain and matched reasonably well with model results (Clement et al., 2000). Whereas the Lake Pallcacocha record has served as an authoritative benchmark for many Paleo-ENSO studies (e.g. Beck et al., 2017), several authors have pointed to appreciable differences between the Pallcacocha record and other Holocene ENSO reconstructions from the Central and Eastern Pacific (Baker and Fritz, 2015; Chen et al., 2016; Cobb et al., 2013; Zhang et al., 2014). Moreover, inconsistencies exist with hydroclimatic reconstructions from Peru (Bustamante et al., 2016). Important differences between the Pallcacocha record and other ENSO reconstructions were also found for the last millennium (Emile-Geay et al., 2013) and discrepancies exist with ENSO reconstructions covering the documentary period since AD 1525 (Gergis and Fowler, 2009). Thus, the question arises: what does the Pallcacocha record really show?

Recently, a much more detailed picture of the spatial representation of ENSO-related precipitation became available for Ecuador. Vuille et al. (2000) concluded that, in the Ecuadorian Andes 1–4° S, it is rather the cold ENSO phase (La Niña) that is associated with above normal monthly precipitation. Just the reverse is the case for the Pacific coastal plains. Despite noticing a weak non-significant increase in austral summer (DJF) precipitation for El Niño years on the western slope of the Andes between 0 and 3°S (Vuille et al., 2000), El Niño is typically characterized as drier in the Andes. For the western slope of the Andes 1–3°S, Vuille et al. (2000) noted that "…the highest precipitation was received during an El Niño (1982/83), a La Niña (1988/89), and a 'normal' year (1969/70)". The finding of generally wetter conditions in the Andes during La Niña was further backed up by daily maximum river discharge (Ward et al., 2010), although the relation was significant only in DJF. In the most comprehensive analysis of monthly homogenized precipitation data from Ecuador, Vicente-Serrano et al. (2017) concluded that precipitation across the Ecuadorian Andes is mostly above normal during La Niña phases. The authors also noticed a very complex spatial pattern of precipitation in Ecuador with generally opposite signs of the ENSO signal seen in the Andes and the Pacific coast. A significant difference between coastal and Andean precipitation has already been documented by Horel and Cornejo-Garrido (1986; Figs. 10 and 11 therein) for the very strong El Niño 1982/83. Above average precipitation was noted for the coastal plain and the lower part of the western slope whereas precipitation rates did not exceed average values above 3000 m a.s.l. (where Lake Pallcacocha is located) except for a weak positive anomaly in April 1983 (although with low precipitation rates of ca. 30 mm per month). Interestingly, Bendix et al. (2011) reported heavy precipitation and flooding for this area during a typical La Niña year 2008 and they pointed to an important difference between SST anomalies in the Central Pacific (Niño 3.4) and the Eastern Pacific (Niño 1 + 2). Most recent literature (Sulca et al., 2018) confirms that the position of the sea surface temperature (SST) anomalies (central and eastern Pacific) but also the meridional displacement of the Intertropical Convergence Zone (ITCZ, central or eastern Pacific) modulate the spatial pattern of precipitation in Ecuador. The area of Lake Pallcacocha seems to be in the transitional zone where correlations between ENSO with different flavors and precipitation change sign and, thus, heavy precipitation may occur during all ENSO phases (Vuille et al., 2000).

It appears that the conclusions drawn from regional instrumental monthly meteorological data are in conflict with the El Niño-interpretation of the clastic laminae in Lake Pallcacocha (Moy et al., 2002; Rodbell et al., 1999). As Lake Pallcacocha sits at a very high elevation in the Andes (4050 m a.s.l.) but only one kilometer east of the water divide of the Western Cordillera, it is not clear which rainfall domain Lake Pallcacocha belongs to. Accordingly, the interpretation of the Pallcacocha sediment record has wide implications for the general understanding of Holocene Paleo-ENSO.

In this article, we revisit the Pallcacocha flood layer record in light of new local and regional daily precipitation data that were not available to Rodbell et al. (1999). First, we present an independent flood layer record from Lake Pallcacocha and compare it with a new flood record from adjacent Lake Fondococha where similar clastic layers were discovered. We assess whether the Pallcacocha flood record from Rodbell et al. (1999) and Moy et al. (2002) can be reproduced from a different coring site in the same lake and from a nearby lake in the same region. In our analysis, we focus on the last 1000–1500 years, a period for which several independent ENSO reconstructions and other paleoclimate information exist (PAGES 2k Consortium, 2013; PAGES 2k Consortium, 2017). Second, we analyze local and regional daily rainfall data to assess the synoptic-scale weather patterns that lead to intense precipitation at Lake Pallcacocha, and we investigate whether or not intense precipitation in this area is related diagnostically to El Niño conditions (cf. Rodbell et al., 1999).

2. Regional setting

Cajas National Park (CNP) (2°50′S; 79°10′W; Fig. 1a) is located mainly on the eastern slope of the Western Cordillera in the Ecuadorian Andes. The park comprises an area of about 285 km^2 and ranges from 3150 m to over 4400 m a.s.l. (Astudillo et al., 2011). The geology consists mainly of tuff, rhyolite, and andesite from the Pleistocene Tarqui-formation (Paladines et al., 1980). The southeastern border of the CNP belongs to the cretaceous Celica-formation, which is characterized by tuff and andesite. In general, the subsurface landscape is covered by Pleistocene glacial deposits with Holocene Andosols and Histosols as the dominant soil types (Harden, 2006). The Cajas National Park hosts > 240 lakes of glacial origin. At lower elevations, moist montane forest dominates. Páramo grasslands with patches of *Polylepis* extend

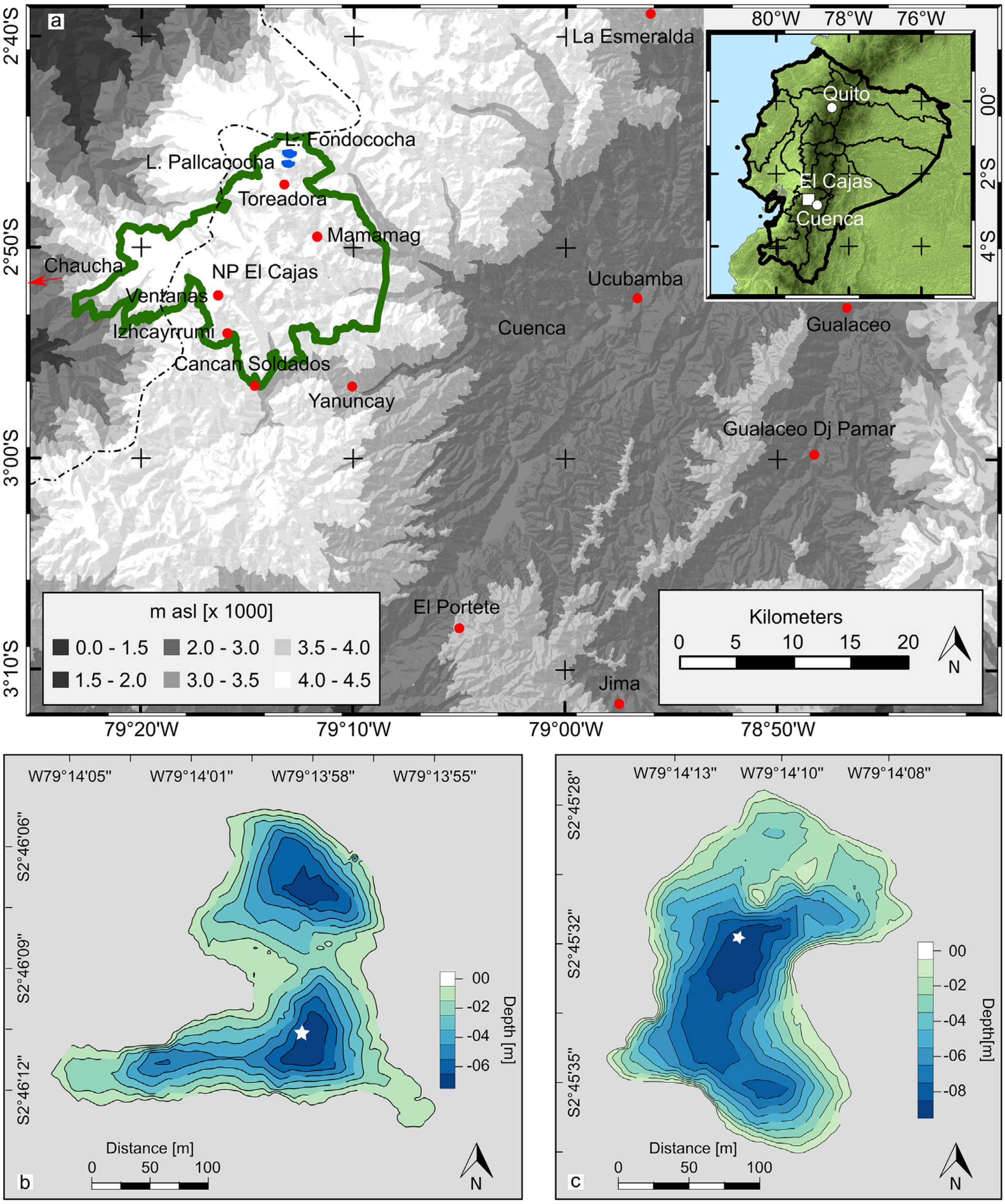

Fig. 1. Site description. (a) Map of El Cajas National Park, SW Ecuador, with the locations of Lake Pallcacocha, Lake Fondococha, and the meteorological stations (red dots, see Suppl. Table 1). The dashed line highlights the water divide. Bathymetric maps are shown for Lake Pallcacocha (b) and Lake Fondococha (c). The white asterisks indicate the coring sites. (For interpretation of the references to colour in this figure legend, the reader is referred to the web version of this article.)

above ca. 3500 m a.s.l., covering 90% of the park area (Hansen et al., 2003; Wille et al., 2002). Whereas the vegetation composition remained fairly stable during the Early Holocene, anthropogenic disturbance has been documented in palynological records from the mid-Holocene onwards and clearly for the past 2000 years (Hansen et al., 2003; Rodbell et al., 2008).

Diurnal temperatures range between 6 and 18 °C in the moist montane forest belt, and vary between 3 and 6 °C in the Páramo and show little seasonal variation (Bandowe et al., 2018). Annual precipitation in the CNP increases with altitude from ca. 700 mm to ca. 1300 mm in the Páramo. Two rainy seasons exist, with one from February to May and one from October to December.

Fig. 1b–c show the two case study lakes, Lake Pallcacocha (PAL, 4050 m a.s.l., Fig. 1b), and Lake Fondococha (FON, 4130 m a.s.l., Fig. 1c). Lake Fondococha was selected because it is very close to Lake Pallcacocha (< 1.2 km), at comparable elevation, and the sediments exhibit numerous clastic laminae similar to those described by Rodbell et al. (1999). Both lakes are of glacial origin (Rodbell et al., 2008). The lakes are exorheic, polymictic and oligotrophic systems located in the Páramo grassland at around 4100 m a.s.l., between 3 and 5 ha in size and between 8 and 10 m deep with slightly alkaline waters.

3. Methods

3.1. Sediment analyses

In July 2014, multiple short (< 1.5 m) sediment cores were retrieved at the depocenter of the lakes (Fig. 1) using a UWITEC gravity corer and transparent core liners to verify that the surface sediment was not disturbed during coring. The cores were first scanned for magnetic

susceptibility and density with a Multi-Sensor Core Logger (MSCL, Geotek) at 1 cm resolution (Schultheiss and Weaver, 1992) and then sedimentologically described (Schnurrenberger et al., 2003). One core half was scanned with a SPECIM Ltd. VNIR hyperspectral imaging scanner for sediment colour in the visible and near infrared (VNIR) range (Butz et al., 2015) and with a µXRF ITRAX scanner for elemental composition (Croudace et al., 2006) using a Mo-tube (resolutions = PAL: 0.5 mm; FON: 1 mm). The µXRF settings included exposure times at 10 s, voltage at 30 kV and current at 35 mA (FON) and 40 mA (PAL). RGB (red-green-blue) scans and X-radiography density measurements were taken (resolution = 0.2 mm) and linearly interpolated to the µXRF data resolution.

^{210}Pb and ^{14}C chronologies were established with sample material from the other core halves. The top ~30 cm were contiguously subsampled at 0.5 cm resolution and freeze-dried. Activity measurements were performed by gamma spectrometry for ^{137}Cs and ^{226}Ra, and alpha spectrometry for ^{210}Po (Tylmann et al., 2016) at the University of Gdansk, Poland. ^{210}Pb-ages were modeled with the Constant Rate of Supply (CRS) model (Appleby, 2008; von Gunten et al., 2009), with and without removal of clastic layers (Arnaud et al., 2002) and tested for missing $^{210}Pb_{unsupp}$ inventories (Tylmann et al., 2016). Despite extended counting time, ^{137}Cs activities were mostly below detection limits except for a few samples. In the lower part of the core, parallel ^{14}C-AMS measurements were performed on terrestrial plant microfossils and bulk sediments to assess potential ^{14}C reservoir effects (Geyh et al., 1999). Terrestrial plant macrofossils were prepared after wet sieving (100 µm) of contiguous sediment slices at 1 cm resolution (1 cm corresponds to 10–20 years resolution, see Section Results). Macrofossils were taxonomically identified and dated with the ^{14}C AMS MICADAS system at the University of Bern (Szidat et al., 2014). Miniature samples (< 420 µg carbon) were dated with direct gas injection (Salazar et al., 2015). The radiocarbon-ages were calibrated with the IntCal13 calibration curve (Reimer et al., 2013). Bayesian age-depth modeling ("rbacon" package v2.3.4, Blaauw and Christen, 2011, 2018) was applied to calculate age-depth models (initial parameters can be found in Suppl. Table 3). Clastic layers that resulted from rapid sedimentation were omitted from the sediment stratigraphy for the age-depth modeling using "rbacon-slumps"- feature.

Following Schillereff (2015), we used two independent methods for the identification and classification of clastic sediment layers (flood layers): (i) visual inspection supported by smear slide analysis and (ii) statistical classification of the µXRF, RGB and X-ray density data. Detection of flood layers with µXRF is a widely applied technique (e.g. Wilhelm et al., 2016). These data were scaled (0–1) and subjected to a principal component analysis (PCA) and kmeans-clustering. Significant PCs were identified with the broken-stick approach, and silhouette plots were made to support the choice of the number of clusters used. Both methods were computed using the "stats" package v.3.2.5 (R Core Team, 2016) and silhouette plots were drawn using the "factoextra" package v.1.0.4 (Kassambara and Mundt, 2017) in R. The significant PC-scores were colored section-wise according to the kmeans-cluster, and plotted on false colour contrast enhanced images (VNIR). Three people counted and measured the layers visually on these images using CooRecorder v.2.3 software (Larsson, 2003). Finally, we used the age-depth models to assign ages to the individual clastic deposits, and computed the frequency of clastic layers (flood frequency) using 100-year moving windows. The sum of layers per 100 years is plotted at the midpoint of the window.

Eight thick lithoclastic layers of Lake Pallcacocha were investigated for detailed stratigraphy, water content (Håkanson and Jansson, 2002), total organic carbon (Loss on Ignition 550 °C; Heiri et al., 2001), grain size distributions (Malvern Mastersizer 2000s), elemental (ITRAX XRF scanner) and mineralogical composition (XRD).

3.2. Analyses of meteorological data

24 h and 72 h precipitation sums from nine weather stations with daily observations (Fig. 1a) were investigated in order to identify dates with heavy precipitation. This was used to assess the synoptic atmospheric circulation patterns that lead to strong surface runoff, potential alluvial activity in the watershed, and the formation of clastic layers in the lake sediments. Suppl. Table 1 summarizes the coordinates of the stations, the lengths of the data series, and the sources of the raw data. Seven stations cover the years 2002 to 2016, and the shortest record (Toreadora) spans only December 2012 to July 2016. But this station is closest to the lakes. The longest record (Gualaceo station) covers the years 1964 to 2012 but is 50 km to the east. First, we defined intense 24 h and 72 h precipitation by three percentiles ($P_{0.95}$, $P_{0.99}$, and $P_{0.995}$) and classified the corresponding dates at every station individually. Afterwards, we searched for intense precipitation events that were registered in at least four stations simultaneously (data coverage 2002–2016) in order to place more weight on spatial coherency. For each station, annual precipitation cycles were plotted from the monthly precipitation sums (two examples given in Suppl. Fig. 4, rest not shown).

The individual dates with observed extreme precipitation (24 h and 72 h precipitation, one or four stations, three different percentiles) were then compared with 15 different ENSO indices (monthly data; references in Suppl. Table 2). Every observation of an extreme precipitation event was assigned to an ENSO-phase (La Niña, El Niño, or Neutral). We repeated all calculations for a lag −1 month to test for delayed precipitation responses to ENSO.

The synoptic evolution of each extreme precipitation event (± 3 days) was examined with daily NCEP/NCAR Reanalysis 1 data (Kalnay et al., 1996). We investigated windfields and relative humidity at different pressure levels (300 hPa and 500 hPa) and calculated mean charts that included all of the intense precipitation events (24 h, 72 h, $P_{0.95}$, $P_{0.99}$, and $P_{0.995}$) per station.

In addition and only for qualitative comparison, we added daily precipitation data from five nearby stations that were installed in 2014, including one on the western slope at high elevation. Although the records are very short they cover the strong El Niño 2015/16.

4. Results and interpretation

4.1. Sediment stratigraphy

Fig. 2 shows the sediment cores of both lakes and the classification into two major lithotypes. In Lake Pallcacocha, lithotype 1 (LT1) consists of massive olive brown (2.5 YR 4/4) to dark olive brown (2.5 Y 3/3) organic silty clay (silty loam) with up to 17% C_{org} and high water contents (60–80%). The sediment is rich in phytoliths, diatoms, and grains of volcanic tephra. The organic matter is strongly decomposed and amorphous. Lithotype 2 (LT2) consists of clastic silty-clay laminae that are 1 to 30 mm thick and bright yellowish brown (2.5 Y 6/8; 2.5 Y 7/8) in colour. The mineral fraction of these laminae is composed of 25% quartz, 15% plagioclase, and 60% phyllosilicates. Compared to LT1, the C_{org} content is lower (generally < 6%), the X-ray density is higher, and the water content is lower (40–65%). The clastic layers are also enriched in elements that exhibit affinity to lithogenic components (Zr, Rb, Sr, Si among others; Fig. 2). Lithotypes 1 and 2 are very similar in Lake Fondococha.

Fig. 2 shows the classification of the clastic layers using both approaches: (i) the visual classification and (ii) the PCA of the combined RGB, X-ray density and µXRF data (K, Rb, Si, Ti, Sr, Zr). The broken stick models show that only the first principal component (PC1) is significant: PC1 explain between 63% and 72% of the variance in the two lakes. Visual clastic layers (LT2) in the top ca. 10 cm of the cores are absent in both lakes. The very fine laminations visible in the NIR picture of the top section of Lake Pallcacocha (Fig. 3a) show that the

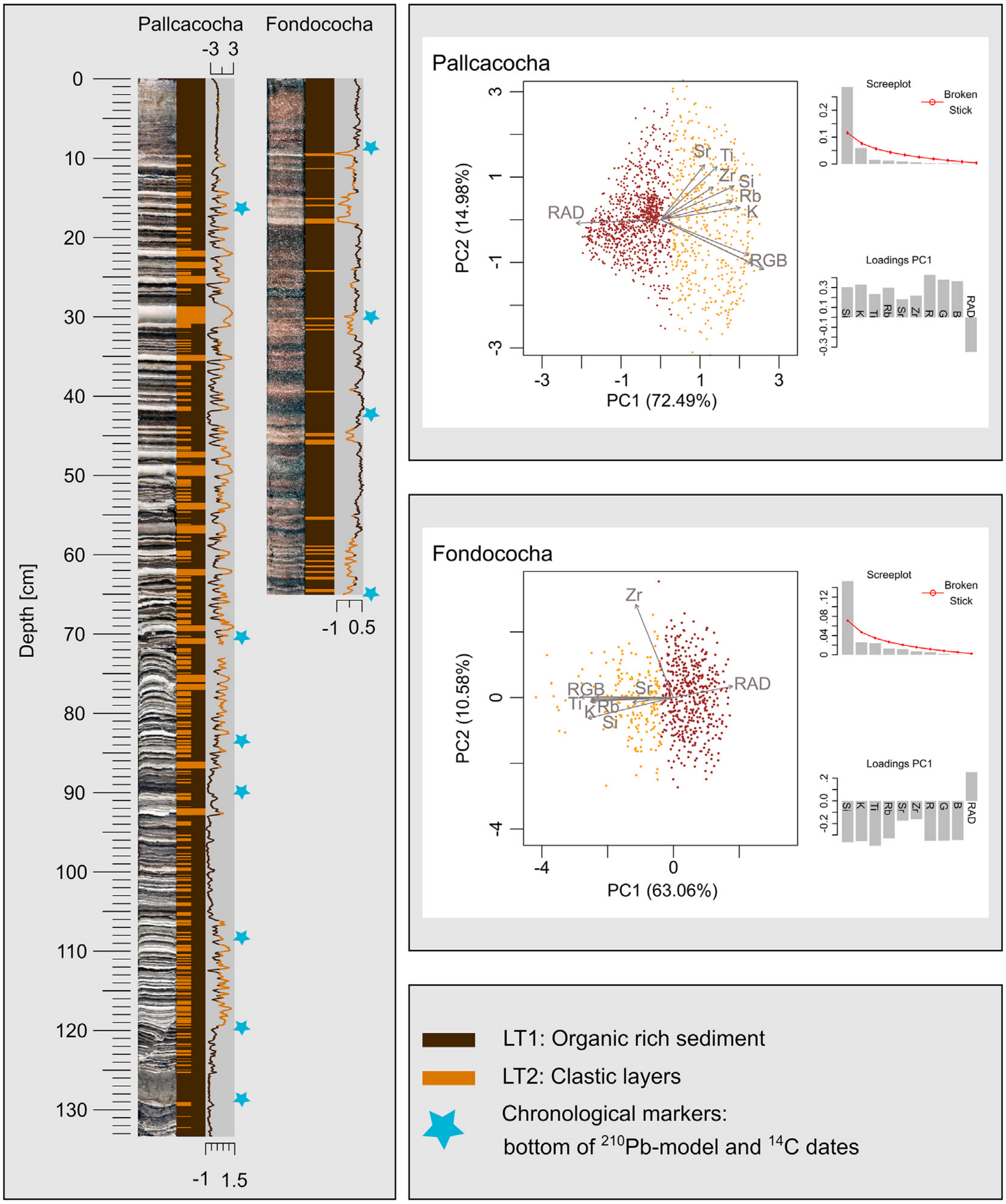

Fig. 2. Sediment cores overview and sediment classification. Sediment cores of Lake Pallcacocha and Lake Fondococha showing the false colour (NIR) contrast enhanced core pictures (left), the visual classification of organic Lithotype LT1 (dark brown) and clastic Lithotype LT2 (light brown), and the statistical classification (PC1, k-means clusters for LT1 dark brown, and LT2 light brown). The biplots, screeplots and the loadings of the PCA of each core are shown on the right. (For interpretation of the references to colour in this figure legend, the reader is referred to the web version of this article.)

sediment was not mixed during coring or transport. In contrast to the topmost part of the cores, clastic layers cluster in groups or appear individually throughout the rest of the sediment sequences. Within the lakes, the clastic layers can be stratigraphically correlated across parallel cores, suggesting that the stratigraphy of the clastic layers (LT2) in the individual lakes is reproducible.

Eight clastic layers (LT2) from Lake Pallcacocha were investigated in detail with 3–4 subsamples per clastic layer (not shown). They show sharp (< 1 mm) non-erosive basal contacts and upward fining of the grain size distributions: clay increases from ca. 10% to > 50% whereas silt decreases from > 80% in the basal stratum to < 40% at the top (clay cap). Ti, Sr, and Si concentrations decrease with declining silt content, whereas K increases with higher clay content towards the top. The internal structure is similar in all eight clastic layers that were investigated in detail.

We interpret the origin of the clastic layers with the non-erosive basal contacts and the upward fining of lithogenic material to be rapid depositions from episodic hyperpycnal flows (undercurrents or interflows) with high loads of suspended sediment.

4.2. Chronology

Three ^{210}Pb age-depth models for Lake Pallcacocha and the ^{14}C chronologies for both lakes are shown in Fig. 3a-c. The different variants (with and without flood layer removal and missing inventory correction, data not shown) of the ^{210}Pb age-depth model suggest that the homogenous top part of the sediment (0–9 cm) covers the last ca. 40–50 years and that the first clear flood layer at 9.5 cm sediment depth

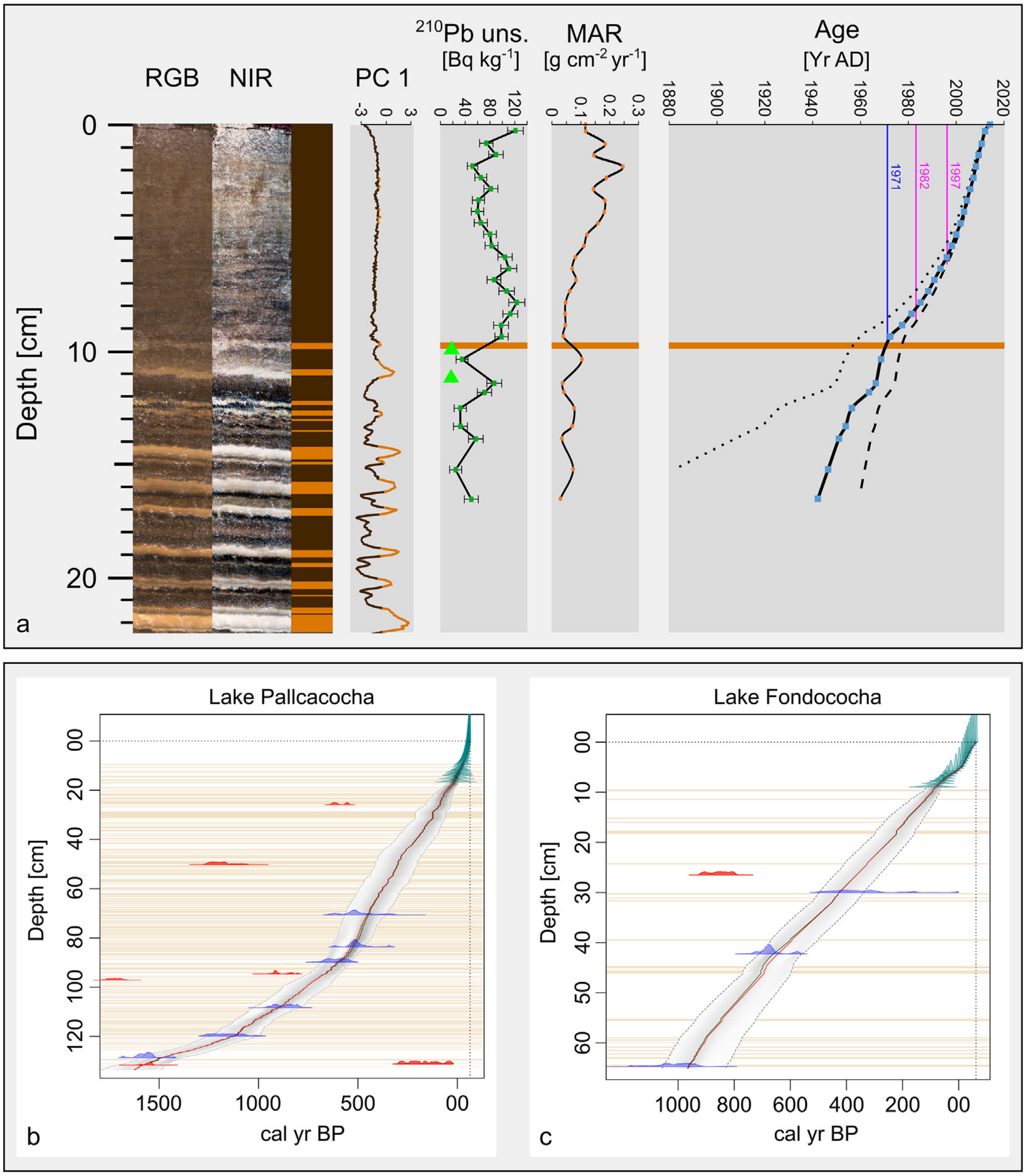

Fig. 3. Chronologies. (a) Shows the RGB and NIR close-up pictures of the topmost 22 cm sediments of Lake Pallcacocha with the sediment classification (PC 1), the ^{210}Pb and ^{137}C activities (green triangles), the MAR, and three different CRS age models with flood layers removed (dotted line: no missing inventory correction, solid line: missing inventory correction fitted through samples below 7.85 cm, the selected one, and dashed line: missing inventory correction starting at 13.85 cm, magenta vertical lines indicate the EN years 1982/83 and 1997/98, the blue vertical line indicates the age of the first "classic" flood layer). Light brown boxes indicate the first "classic" flood layer at 9.5 cm sediment depth. (b-c) show the combined (^{210}Pb and ^{14}C, green and blue/red) bayesian age-depth models for (b) Lake Pallcacocha and (c) Lake Fondococha. Red lines represent the mean age (used for calculations) and green lines indicate the median ages. The clastic layers (light brown) were removed prior to age modeling. The AMS ^{14}C dates on bulk organic matter and insect chitin (red) show substantial ^{14}C reservoir effects and were not used to establish the chronology. (For interpretation of the references to colour in this figure legend, the reader is referred to the web version of this article.)

was deposited between ca. 1965 and 1975 (range of ca. 10 years with five models), but not younger than 1980 (most extreme model). All models suggest that the sediment corresponding to 1997/98 (year with strong El Niño) falls between 5 and 6 cm sediment depth. Age uncertainties spread considerably below 10 cm (prior to ca. 1970) and are not further used here. Detectable ^{137}Cs was found between 9.5 and 10.5 cm sediment depth, which corresponds to ca. 1960–1970 according to the ^{210}Pb age profiles.

Sediment sieving revealed that terrestrial macrofossils suitable for ^{14}C AMS dating were surprisingly rare and small. Most of the sediment organic matter is strongly decomposed. ^{14}C dates on bulk organic carbon and aquatic insect chitin suggest ^{14}C reservoir effects for these materials on the order of 400–600 years. Most of the terrestrial plant macrofossils were identified as *Loricaria sp* (Table 1). Although many of the samples were very small (137–800 µg), ^{14}C dating with direct gas injection revealed consistent ages with acceptable uncertainties (typically SD < 60 yr). The dating uncertainty increased up to 200 years for miniature samples with < 70 µg sample mass.

For Lake Fondococha (Fig. 3c), the BACON-model shows constant sedimentation rates of ca. 6.5 cm/100 yr, and a basal age of ca. 1000 cal yr BP for the 65 cm long core. The top part of the chronology is constrained by ^{210}Pb dates reaching an age of ca. 1880 CE at 8 cm sediment depth. Lake Pallcacocha shows an exponential increase in sedimentation rates from 4 cm/100 yr in the lower part of the core to 10–16 cm/100 yr in the last 500 years (Fig. 3b). Our core from Lake Pallcacocha extends back to ca. 1600 yr BP. Based on the sedimentation

Table 1
Summary of the ^{14}C data showing the Sample ID (PAL = Pallcacocha, FON = Fondococha), sample sediment depth, sample type and mass, the ^{14}C ages, and the calibrated ages.

Sample	Depth [cm]	Material	Tot. weight [mg]	^{14}C yr BP	Error [+/− 1s]	Cal. yr BP [max. prob.]	Min/Max [1s]
PAL14-2-I-B-1_25.7-26.2	**25.95**	**Bulk**	**1115.7**	**572**	**22**	**615**	**591, 639**
PAL14-2-I-B-3_mf	*50.35*	*Insect-Elytra*	*0.8*	*1276*	*48*	*1232*	*1172, 1292*
*PAL-14-2-I-B_69.5-71.6**	*70.55*	*Plant tissue*	*0.137*	*477*	*55*	*498*	*433, 563*
*PAL-14-2-II-A_11-12.5**	*83.75*	*Plant tissue*	*0.128*	*468*	*55*	*495*	*429, 560*
PAL14-2-II-A_17.6-18.4*	**90**	**Fern and Loricaria fragments**	**1.109**	**633**	**81**	**605**	**514, 696**
PAL14-2-II-A-1_22.8-23.3	**95.05**	**Bulk**	**858.3**	**987**	**22**	**928**	**901, 955**
PAL14-2-II-A_25.4-25.9	*97.65*	*Loricaria leaf fragment*	*0.241*	*1786*	*67*	*1699*	*1562, 1836*
*PAL-14-2-II-A_36-37.2**	*108.6*	*Plant tissue*	*0.237*	*969*	*54*	*865*	*761, 968*
*PAL-14-2-II-A_47.6-48.5**	*120.05*	*Plant tissue*	*0.416*	*1231*	*62*	*1169*	*1051, 1287*
PAL14-2-II-A_56.4-57.4*	**128.9**	**Loricaria leaf fragment**	**1.424**	**1659**	**38**	**1573**	**1517, 1629**
PAL14-2-II-A-2_59.6-60.1_bulk	**131.85**	**Bulk**	**670**	**1652**	**23**	**1568**	**1522, 1613**
PAL14-2-II-A-2_59.6-60.1_MF	*131.85*	*Loricaria leaf fragment*	*0.4*	*150*	*36*	*201*	*167, 234*
FON14-2-I-B-1_26.4-26.9	**26.55**	**Bulk**	**963**	**940**	**26**	**858**	**795, 920**
*FON14-2-I-B-2_mf**	*30*	*Seed; Carex tricuspid*	*0.195*	*301*	*62*	*360*	*276, 503*
FON15-tephra(above)_39-41*	**42.25**	**Loricaria leaf fragment**	**1.217**	**726**	**38**	**688**	**648, 728**
FON15-tephra(above)_67-68*	**64.7**	**Loricaria leaf fragment**	**0.619**	**1080**	**51**	**1004**	**919, 1088**

Bold fonts indicate samples that were measured from graphite targets, *italic* fonts indicate samples that were processed using direct gas injection. Asterisks (*) in the column "Sample" mark samples that were included in the final chronologies.

rates, the sampling intervals of 1 cm used for macrofossil sieving translates into an additional maximum age error of 15 years in Lake Fondococha and < 25–30 years in Lake Pallcacocha.

4.3. Flood frequency

The flood stratigraphies, as established with two different detection methods and the sediment chronologies, were used to compute the flood frequency records for both lakes (Fig. 4a–b). With the exception of the period around 1400 CE and 1900 CE to present in Lake Pallcacocha, the statistical and the visual flood layer detection reveal broadly consistent results, suggesting that the results are not influenced by the choice of the flood layer detection method. As outlined above, the individual floods can be stratigraphically correlated in parallel cores from the same lake (data not shown) implying that the history of flood frequency is reproducible for each lake.

Both lakes exhibit strong centennial-scale variability in the flood frequencies, ranging between 1 and 8 clastic layers per 100 years in Lake Fondococha and between 5 and 30 floods per 100 years in Lake Pallcacocha. Overall, and taking into account chronological uncertainties (dating and age modeling), both lakes show some similarities (decreasing trend towards the present) and major dissimilarities. For example, the flood-frequency of Lake Fondococha peaks in the 11th century, whereas in Lake Pallcacocha (our record), it shows low values during that time. In contrast, in Lake Pallcacocha the frequency reaches the highest values at around 1400 AD. The comparison between the different Pallcacocha records (Fig. 4b–e) uncovers many inconsistencies attributable to different chronologies and proxies used to detect event layers. The major common feature is the decreasing trends towards the present as seen in Fig. 4b,d,e, but not in Fig. 4c.

4.4. Synoptic patterns of intense precipitation and its relation to ENSO

The attribution of intense ($P_{0.95}$ and $P_{0.99}$) 24 h precipitation to ENSO positive (El Niño), 'Neutral' and negative (La Niña) phases is shown for the tree closest meteorological stations in Fig. 5 (time series) and Fig. 6a–c (classification). The classification results for all stations and details about the ENSO indices are presented in Suppl. Figs. 1–3, and Suppl. Table 2, respectively.

Toreadora, the station closest to Lake Pallcacocha, covers a short period from December 2012 to December 2016. This period is strongly biased by ENSO positive (EN) conditions (ENSO positive ca. 60–70% of the time, depending on the ENSO index; Suppl. Fig. 1). The ternary classification (El Niño, Neutral, La Niña; Fig. 6a bottom) shows that < 40% of the events occurred during El Niño phases (except for HADISST NIÑO3.4 and NIÑO4 and ERSST NIÑO12 and NIÑO4 ca. 50%) and an equal proportion or even most of the heavy precipitation events occurred during 'Neutral' and La Niña conditions. With a binary classification (ENSO positive/negative, Fig. 6a top) 50–70% of the intense precipitation events at Toreadora occurred during ENSO positive phases. However, if the ENSO positive bias of the observational period is taken into account, then the probability of intense precipitation is about the same for ENSO positive and ENSO negative phases. The time series of the 24 h precipitation sums (Fig. 5a) shows that at Toreadora station, during the super El Niño 2015/16, no unusually intense precipitation was recorded. In contrast, similar precipitation rates were also observed during weak La Niña and 'neutral' phases. The Toreadora station record (2012–2017) does not cover strong La Niña years.

Cancan Soldados and Yanuncay (Fig. 5b and 6b–c) have a longer record (2002–2016) and are also located nearby Lake Pallcacocha. Cancan Soldados is a high elevation station (3500 m a.s.l.) and within 10 km of the Andean water divide, thus most representative for Lake Pallcacocha. The meteorological record shows no bias towards a particular ENSO phase. All ENSO indices show that, overall < 40% of the heavy precipitation event occurred during El Niño events, between 10 and 40% during La Niña events and the majority during 'neutral' phases (Fig. 6b bottom). This picture is confirmed by the time series (Fig. 5b): at Cancan Soldados, the highest precipitation was recorded in April 2014 ('neutral'). Numerous events were also recorded in 2008 (La Niña) and the strong El Niño 2015/16 shows relatively weak precipitation, confirming the inferences from Toreadora station.

The results in Fig. 6 are consistent for all stations using both the binary and ternary classification (Fig. 6 and Suppl. Fig. 3). Similar results are also obtained if the selection includes only precipitation events that were observed simultaneously at least in four, five or six meteorological stations, if intense precipitation is defined as the 72 h precipitation sum, and even for exceptionally strong precipitation ($P_{0.995}$). The findings remain robust if the relation between occurrence of intense precipitation and ENSO phase is computed with a lag of 1 month for precipitation (data not shown).

Station information from the upper western slope is largely missing. The only station available (Chaucha, 1750 m a.s.l., Fig. 5a) provides only a short data series but covers the strong El Niño 2015/16. Fig. 5 shows that the largest precipitation event observed on 19–21 March 2015 (< 130 mm in 72 h), which exceeded all precipitation intensities measured on the eastern slope of the Andes, did actually not reach the area of Lake Pallcacocha and was barely registered at Toreadora station (total 13 mm in 72 h). Precipitation intensities during the peak El Niño

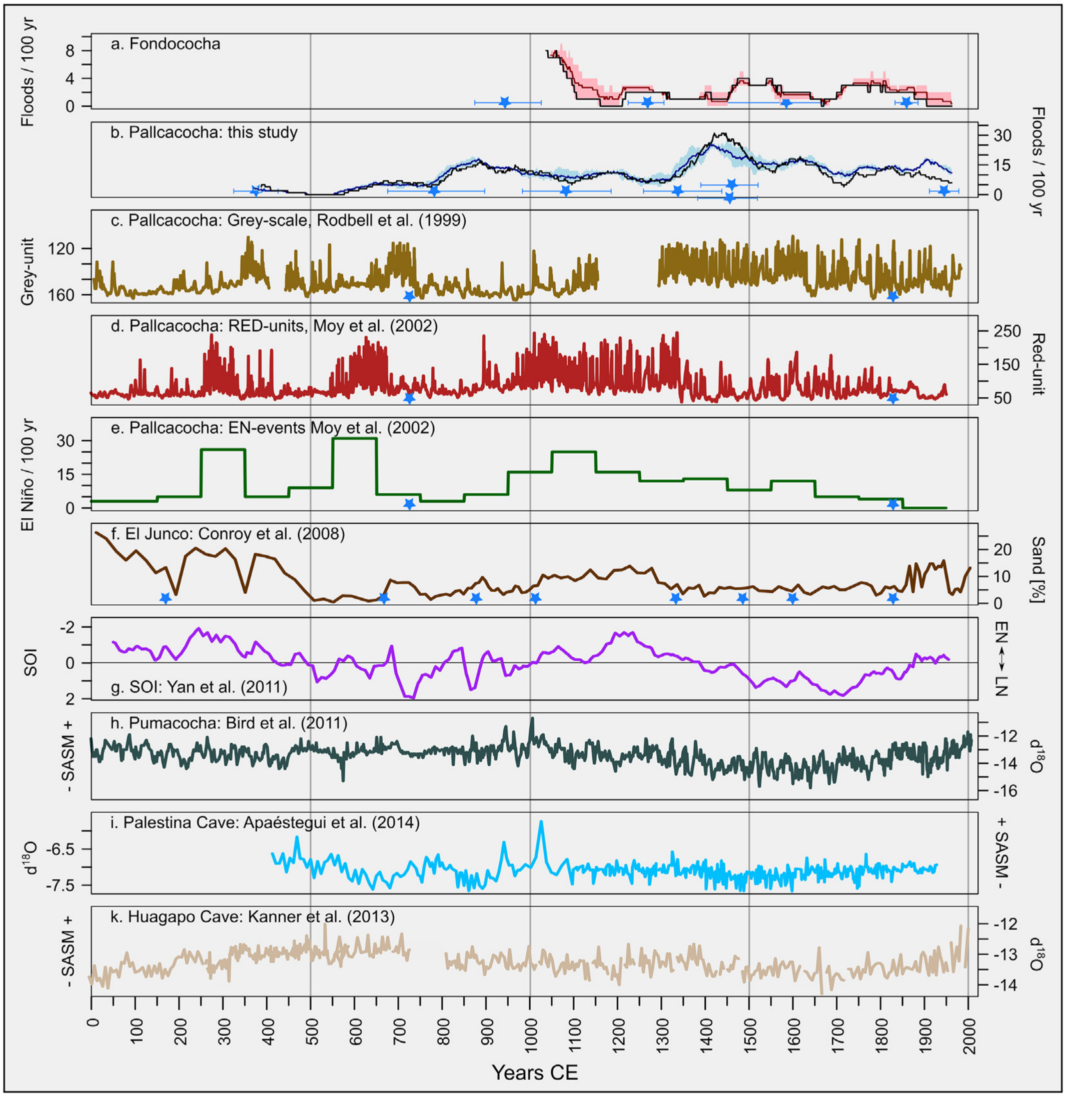

Fig. 4. Comparison of the flood frequencies from the present study with different records. The flood frequencies are shown for Lake Fondococha (a) and Lake Pallcacocha (b). The black lines show the flood histories from the PCA and k-means discrimination. The average of three individual visual counts is shown in the colored lines, and the min/max of visual counts is shown in the shaded range. (c-e) display the flood frequency reconstructions from Rodbell et al. (1999) and Moy et al. (2002), (f) sand content in sediments of El Junco Crater Lake, Galápagos (Conroy et al., 2008); the authors interpret high sand content as more frequent El Niño; (g) SOI-reconstruction (Yan et al., 2011) and (h) South American Summer Monsoon SASM reconstructions from Lake Pumacocha, Peru (Bird et al., 2011), (i) Palestina Cave (Apaéstegui et al., 2014) and (k) Huagapo Cave (Kanner et al., 2013). Asterisks denote chronomarkers in the Ecuadorian and Galápagos lakes. The data from c-k was downloaded from the NOAA paleoclimatology data server.

(June 2015–May 2016) were generally low.

In order to detect the moisture sources and synoptic patterns leading to intense precipitation in the region, we computed composites from NCEP/NCAR Reanalysis 1 data for the days of the events. Fig. 7 shows the wind-field and relative humidity at 500 hPa for the 159 intense 24 h precipitation events ($P_{0.99}$) registered at Gualaceo station (data 1964–2012). The synoptic analysis shows that, before and during intense precipitation events, easterly winds prevail and relative humidity is higher on the eastern side of the Andes than on the western side. Orographic effects are also visible, with drier air in the lee of the Andes towards the Pacific coast. We computed the same composites for all seven stations individually, for 24 h and 72 h events at different thresholds ($P_{0.95}$, $P_{0.99}$, $P_{0.995}$), and for the 300 hPa and 500 hPa pressure levels. All combinations produced similar results with predominantly easterly flow.

Observational hourly wind data are available from Toreadora station for one year (July 2014–July 2015). All six case study events ($P_{0.99}$) during this period reveal predominantly E and SE flow during the days of the intense precipitation events and during the hours with rainfall (data not shown). Southerly flow is observed during a few hours only.

5. Discussion

Overall, the sediments of both lakes are very similar. The organic-rich fine-grained matrix (lithotype LT1) is interpreted as continuous sedimentation in a very calm environment. The richness in phytoliths, combined with the nutrient-poor lake water, suggest mostly allochthonous sources of the sediment with substantial additions of soil carbon from the Andosols and Histosols in the catchment. The detailed analysis of the clastic layers (LT2) in Lake Pallcacocha supports the findings by Rodbell et al. (1999) who interpreted the clastic layers as deposits from hyperpycnal flows (Schillereff et al., 2014) related to alluvial activity in the catchment. Given the similarity of the clastic layers in Lake Fondococha to those in Lake Pallcacocha, we interpret all as ‘flood layers’ with rapid sedimentation after alluvial activity in the catchment.

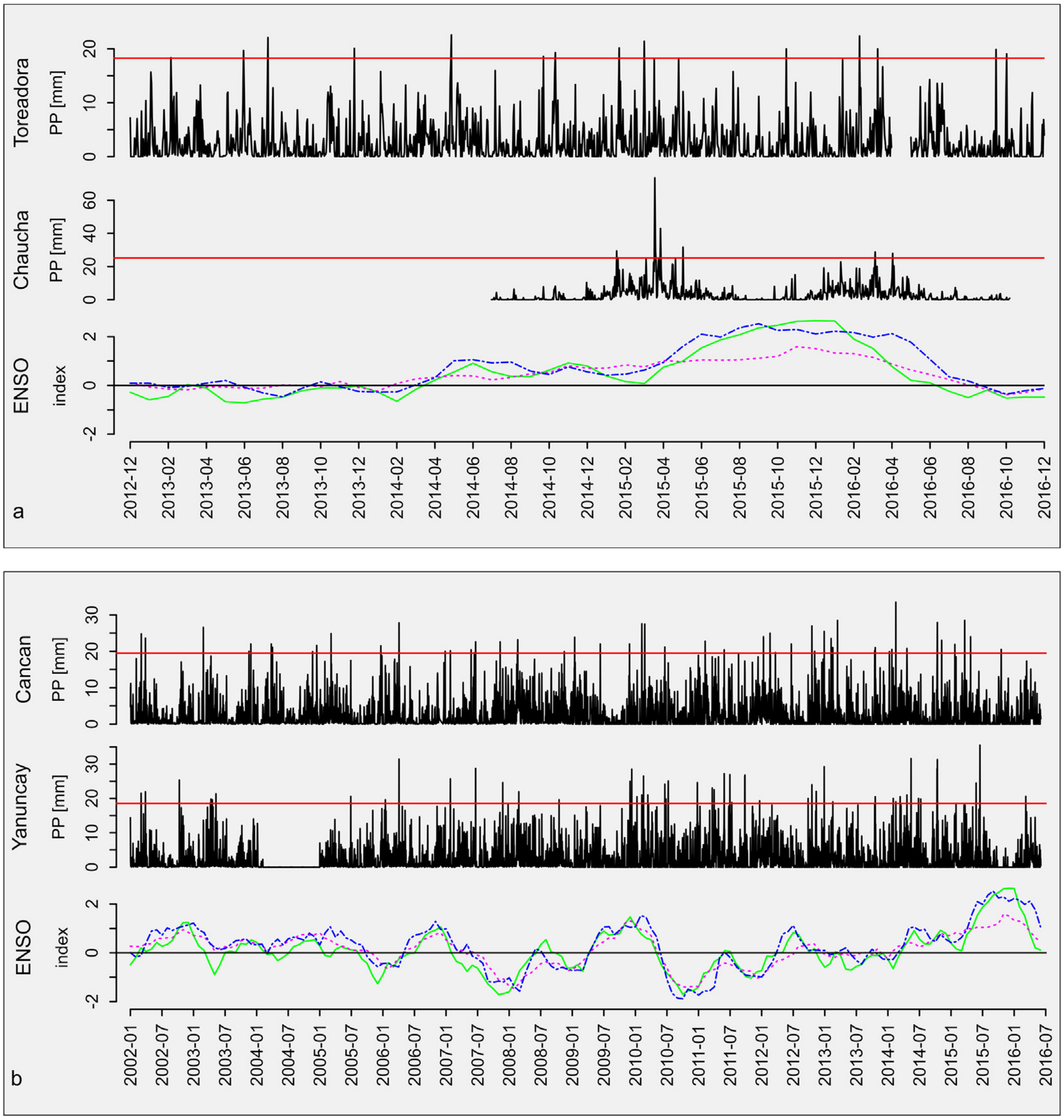

Fig. 5. Time series of 24 h precipitation data of four weather stations plotted along three different ENSO indices. (a) Time series of Toreadora station (nearby Lakes Pallcacocha and Fondococha, top), Chaucha station (west of water divide, middle), and three ENSO indices (bottom): HADISST NIÑO12 (green solid), HADISST NIÑO3.4 (magenta dashed), MEI (blue, dotdashed). (b) Time series of Cancan Soldados station (nearby study lakes, top), Yanuncay station (nearby study lakes, middle) and three ENSO indices (bottom, code as in a). The red horizontal lines indicate $P_{0.99}$. (For interpretation of the references to colour in this figure legend, the reader is referred to the web version of this article.)

For flood frequency reconstructions, precise identification of flood layers remains a challenging task. Following Schillereff et al. (2014) we tested two different approaches and found that the visual inspection and statistical classification of multiple proxies (mainly µXRF, X-ray density, RGB) produced reproducible results in Lake Fondococha (Fig. 4). In Lake Pallcacocha, the two methods of flood layer identification differed slightly in few parts of the core. For instance, at around 110 cm sediment depth, the PCA (mainly through the µXRF data) suggests clastic layers instead of organic sediment (LT 1). The organic sediments in this part contain sand-silt particles that were, however, not transported by hyperpycnal flows and do not classify as LT 2. We consider aeolian processes as a possible transport mechanism for the sand grains in the organic matrix.

^{210}Pb dating is challenging because independent chronostratigraphic markers are lacking. ^{137}Cs is barely measurable in this part of the world (Bandowe et al., 2018; Gunkel, 2003). However, detectable ^{137}Cs was found at around 10 cm sediment depth corresponding to the peak fallout in the 1960s. This is consistent with ^{210}Pb model ages (3 model options) ranging between ca. 1965–1975 for the youngest clear clastic layer at 9.5 cm depth (Fig. 3a). In Lake Pallcacocha, CRS-model-inferred sediment mass accumulation rates are about 1.5 times higher than in Lake Fondococha (Bandowe et al., 2018). This factor compares well with the overall ^{14}C chronology suggesting that the ^{210}Pb age-depth model in Lake Pallcacocha is plausible. We note that, even in the best case, assigning individual (El Niño) years to clastic layers goes well beyond the limits of ^{210}Pb dating.

According to the sedimentology (Figs. 2 and 3) and the ^{210}Pb ages, the uppermost clear clastic layer at 9.5 cm depth predates 1980 (most likely age ca. 1970). In consequence, neither the strong El Niño 1982/83 nor the strong El Niño 1997/98 produced a 'classic' clastic layer as observed further down in the core. It is well possible that some of the faint laminations of the past 40 years fall into these particular El Niño years, but the faint laminations are not unusual.

^{14}C datable and taxonomically identifiable terrestrial macrofossils were difficult to find in both lakes. Although novel technologies with direct gas injection (Salazar et al., 2015) allowed us to process samples with a mass as small as 200 µg, the dating uncertainties of the sediment chronologies remain in both lakes on the order of ± 50–120 years. It

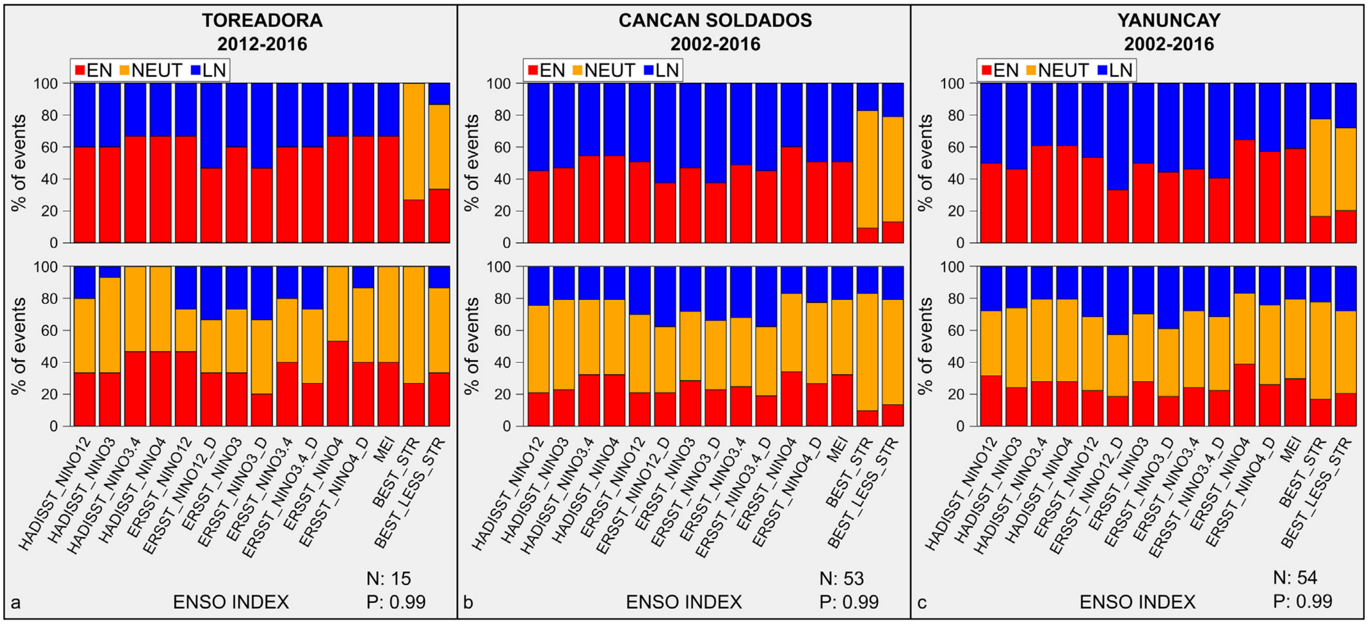

Fig. 6. Barplots showing the proportions of intense 24 h precipitation coinciding with El Niño (EN, red, ENSO positive), 'neutral' (NEUT, orange) and La Niña (LN, blue, ENSO negative) phases displayed for 15 different ENSO indices (monthly values) at three meteorological stations in Cajas National Park, on top the binary classification (EN > 0 > LN) and on the bottom the ternary classification (EN > 0.5 > NEUT > -0.5 > LN) for (a) Toreadora, (b) Cancan Soldados, (c) Yanuncay. N indicates the number of events that exceeded $P_{0.99}$. The plots for all other stations are shown in Suppl. Fig. 3. (For interpretation of the references to colour in this figure legend, the reader is referred to the web version of this article.)

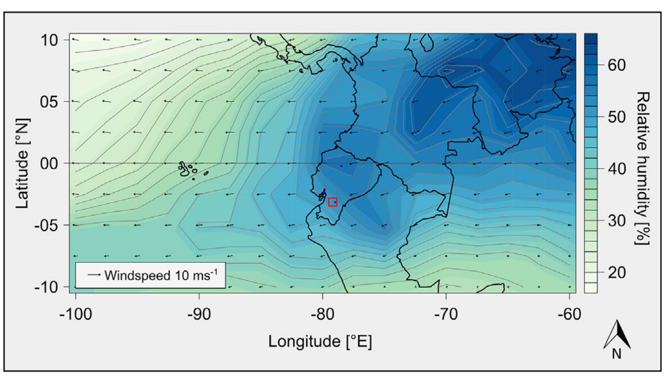

Fig. 7. Synoptic composite integrating all 24 h intense precipitation events registered at Gualaceo station. Wind direction (arrows), wind velocity (arrow-length), and relative humidity in % (contours) at the 500 hPa pressure level are computed from 159 intense 24 h precipitation events ($P_{0.99}$) recorded at Gualaceo. The red square displays the location of the Cajas National Park. Data for the composite plot are from NCEP/NCAR Reanalysis 1 data (Kalnay et al., 1996). (For interpretation of the references to colour in this figure legend, the reader is referred to the web version of this article.)

should be noted that the chronologies and related uncertainties are relevant for assessing if flood frequency reconstructions across sites are consistent. Our flood frequency reconstructions for Lake Pallcacocha and Lake Fondococha (Fig. 4) differ appreciably from the reconstructions by Rodbell et al. (1999) and Moy et al. (2002) (whose reconstructions also differ from each other, Baker and Fritz, 2015). The largest difference is the millennial trend: whereas Moy et al. (2002) reported a decreasing trend from the 11th to the 15th century, our reconstructions suggest rather an increasing trend for this period. It should be noted, however, that Rodbell et al. (1999) did not focus on the late Holocene. Their age model is constrained by only one ^{14}C date for the period considered here, and they used a different model to interpolate between ^{14}C dates. Moreover, the complex bathymetry of Lake Pallcacocha (Fig. 1b) might, at least partly, explain discrepancies between sediment records from different coring sites. Other sediment features seem to be reproducible, such as the absence of clastic layers in the top sediment (Rodbell et al., 1999) despite very strong El Niño events in 1982/82 and 1997/98. Whereas Rodbell et al. (1999) attributed the homogenous top sediments to disturbance during coring, our data (fine laminations, ^{210}Pb profiles) show that this is a true feature reproduced in two lakes.

The absolute flood frequencies are different in Lake Pallcacocha (one event every 3–20 years) and Lake Fondococha (every 12– > 50 years). This is not unusual and suggests that alluvial activity and related hyperpycnal flows are a combination of an atmospheric trigger (intense precipitation) and the catchment sensitivity to runoff and erosion (Brisset et al., 2017). The sensitivity to runoff is mainly defined as a threshold of precipitation at which alluvial activity starts. Whereas the clastic layers in Lake Fondococha register precipitation events that occur with a return period of ca. > 12 years, the layers in Lake Pallcacocha record events with a return period of ca. 3–20 years. Rodbell et al. (1999) observed the typical ENSO frequency band of clastic layers in Lake Pallcacocha, and this is an important element of their argument. However, as Lake Fondococha and Lake Pallcacocha are exposed to the same atmospheric phenomena it is mostly the sensitivity of the catchment that makes the difference in the frequency band of alluvial activity recorded. This may or may not be in the typical ENSO band.

More generally, it is unclear whether or not the frequency band (return period) of alluvial activity alone (i.e. without the demonstrated diagnostic association of heavy precipitation with El Niño events) can serve as diagnostic for ENSO events. Wilson et al. (2010) noted that Holocene ENSO reconstructions yield conflicting results although individual time series show the typical spectral properties of ENSO. The fact that several flood records in Europe also show spectral properties in the 3–12-year domain (Amann et al., 2015 and references therein, Brisset et al., 2017 and references therein) suggests that 'ENSO-like spectral properties' may occur in records that are, in fact, unrelated to ENSO. As a consequence, we advocate that, unless a mechanistic relation between El Niño and alluvial activity can be demonstrated with instrumental data for a given record, the 'ENSO type spectral properties' of such a record might reflect a False Positive.

The analysis of daily intense precipitation in the region of Cajas National Park (including the strong 2015/16 El Niño) shows that there is no diagnostic relationship between the occurrence of potential triggers of alluvial activity (intense precipitation) and ENSO phases. The local and regional meteorological stations demonstrate that intense precipitation occurs at roughly equal probability during El Niño, Neutral and La Niña phases. This observation is supported by earlier findings of Vuille et al. (2000) and Bendix et al. (2011). The latter reference describes the dynamics of heavy precipitation in this area during La Niña 2008. In our data we do not find evidence that support and demonstrate a diagnostic relation between heavy precipitation and El Niño. Instead, heavy precipitation may occur at any time.

In the stations with meteorological data from 2002 to 2016, the strongest relationship between intense precipitation and ENSO positive conditions is found for the Niño4 index. This is surprising, as Vicente-Serrano et al. (2017) found that Niño3.4 best explains hydroclimatic variability in the Ecuadorian Andes, whereas Niño1 + 2 best explains variability in the Pacific coastal plains. Bendix et al. (2011) concluded that heavy precipitation on the coast and in the Andes during 2008 is related to a decoupling between Niño4 and Niño1 + 2 between 2001 and 2009. Also, Sulca et al. (2018) report that ENSO-related precipitation in Ecuador is modulated by the position of the warm pool in the tropical Pacific and the meridional displacement of the ITCZ. In their study, the area of Lake Pallcacocha appears in a transition zone and the relation between precipitation and El Niño (in its different flavors) is not clear.

Multiple testing with different stations, combinations of stations, different rainfall intensities, and different ENSO targets with and without lag-1 month shows very consistent results. A comparison between monthly precipitation data and our selection of dates with intense daily precipitation shows that intense daily precipitation mostly occurs during months of above average precipitation (e.g. relatively wet months; Suppl. Fig. 4). This implies that the findings drawn from monthly precipitation data (Morán-Tejeda et al., 2016; Vicente-Serrano et al., 2017; Vuille et al., 2000 are also largely valid for daily data (our analysis): an association of intense precipitation/wet months and El Niño conditions is not supported in the Ecuadorian Andes at high elevation (including the area of Lake Pallcacocha).

How are the last three very strong El Niño events recorded in this area? Analyzing a transect from the coast to the water divide in the Andes and the eastern lowlands, Horel and Cornejo-Garrido (1986, Figs. 10 and 11 therein) report that precipitation rates above 3000 m. a.s.l. (where Lake Pallcacocha is located) did not exceed average values in 1982/83. According to our age-depth model, a 'classic' clastic layer is missing for that period. Little meteorological information is available for the El Niño 1997/98. But again, a 'classic' clastic layer is not found in the sediment record (at ca. 5–6 cm depth, Fig. 3a). Our sediment record does not include the El Niño 2015/16, but all available information from daily meteorological observations show that precipitation was not unusual during this year.

A remaining question includes how the Lake Pallcacocha flood record compares with hydroclimatic records in the South American Summer Monsoon (SASM) domain and other Late-Holocene ENSO records. Fig. 4 shows that the data structure of all records from Cajas National Park (including Lake Pallcacocha) is appreciably different from the SASM reconstructions from Northern Peru (Lake Pumacocha, Bird et al., 2011) and the regional speleothem records (Apaéstegui et al., 2014; Bustamante et al., 2016; Kanner et al., 2013). Moreover, we agree with Wilson et al. (2010), Braconnot et al. (2012), Emile-Geay et al. (2013), Cobb et al. (2013), Zhang et al. (2014), Baker and Fritz (2015) and Chen et al. (2016), that the currently available ENSO records from Ecuador and the tropical Pacific (e.g. Galápagos) do not provide coherent reconstructions.

We point out that most of the meteorological data used in our study were not available to the pioneers who investigated Lake Pallcacocha (Hansen et al., 2003; Moy et al., 2002; Rodbell et al., 1999).

Our results suggest that the Pallcacocha record should not be used as a benchmark for (late) Holocene ENSO reconstructions. It should be noted, however, that our analysis is restricted to the instrumental period and the last 2000 years. It is, in theory, possible that (i) the relation between alluvial activity, intense rainfall, and ENSO phases was very different in the past, and that the modern analogue (instrumental period) is no longer valid, (ii) the Pallcacocha record contains a (weak) low-frequency El Niño signal that we were unable to identify and/or (iii) past ENSO teleconnections have changed in a way that makes the seemingly inconsistent reconstructions coherent. At the moment we are not aware of any evidence that would support one of these caveats. Moreover, the principle of the modern analogue is fundamental in paleoclimatology.

6. Conclusion

In our study, we analyzed time series of clastic laminae in sediment records from two glacial lakes in the SW Ecuadorian Andes (Cajas National Park) for the past 1500 years. In addition, we evaluated new daily data of intense rainfall to address two questions: (i) is there a relationship between intense precipitation and ENSO phases in this region and, (ii) do the clastic laminae in Lake Pallcacocha provide a conclusive record of late Holocene ENSO?

From our analyses, we draw the following conclusions:

We support the finding by Rodbell et al. (1999) that the clastic laminae in Lake Pallcacocha are produced by hyperpycnal flows following alluvial activity in the catchment and we postulate the same processes for adjacent Lake Fondococha. However, observations for the formation of the clastic layers (modern analogue) are still missing and the corresponding meteorological boundary conditions (precipitation thresholds) for alluvial activity remain unknown.

Clastic layer identification using both statistical and manual methods yielded, with few exceptions, consistent results. Taking chronological uncertainties into account, the flood frequency histories (clastic laminae per 100 years) from Lakes Pallcacocha and Fondococha provide sometimes comparable results, but they differ appreciably from previous reconstructions, particularly with regard to long-term trends in the past millennium. However, neither the 1982/83 nor the 1997/98 very strong El Niño produced clastic layers comparable to those found in the late Holocene. The reason for this hiatus is unknown.

The analysis of daily precipitation data shows that recent intense precipitation occurred at similar probabilities during El Niño, La Niña and Neutral phases. This result has been tested for robustness and is consistent with existing literature. Neither the literature nor the herein investigated meteorological records provide evidence that the very strong El Niños 1982/83 and 2015/16 were accompanied by anomalously high precipitation. The El Niño 1997/98 is poorly documented in meteorological records. The synoptic pattern of the composite shows easterly flow throughout the troposphere, with moisture advection from the Amazon basin and the northern tropical Atlantic.

In summary, we cannot find evidence supporting the idea that strong precipitation in the area of Lake Pallcacocha diagnoses moderate or strong El Niño conditions. At the current state of research, we suggest not to use the flood record preserved in Lake Pallcacocha to reconstruct El Niño events.

More differentiated diagnostics that take into account the position of the warm pool and the displacement of the ITCZ (sensu Sulca et al., 2018) might reveal more conclusive results. Our findings may help explain why comprehensive multi-site, long ENSO reconstructions yield conflicting results. Nevertheless, we acknowledge the pioneering work of Rodbell et al. (1999). We conclude by supporting Braconnot et al. (2012), who highlighted the need to reinvestigate proxy-climate relationships to work towards better Paleo-ENSO reconstructions.

Declarations of interest

None.

Acknowledgements

The Swiss National Science Foundation grant funded the project 200021_152986. MG designed the research. TS did all the sedimentological and statistical analyses, WT measured the ^{210}Pb and ^{137}Cs profiles and helped on the fieldwork. HH and PM provided the meteorological and limnological data and helped with logistics. MG and TS wrote the paper, all authors commented on the drafts. We thank Petra Kaltenrieder (Institute of Plant Sciences, University of Bern) for the identification of macrofossils for ^{14}C dating and Dr. Daniela Fischer and Flavia Isenschmid for lab assistance with the clastic layers. We further thank Mario Cordova and Rolando Célleri for providing meteorological data. ETAPA EP is acknowledged for granting research permission in the Cajas National Park, logistical support, and providing meteorological and limnologic data. We thank Alena Giesche, the Editor and two anonymous reviewers.

Appendix A. Supplementary data

Supplementary data to this article can be found online at https://doi.org/10.1016/j.gloplacha.2018.06.004.

References

Amann, B., Szidat, S., Grosjean, M., 2015. A millennial-long record of warm season precipitation and flood frequency for the North-western Alps inferred from varved lake sediments: implications for the future. Quat. Sci. Rev. 115, 89–100. http://dx.doi.org/10.1016/j.quascirev.2015.03.002.

Apaéstegui, J., Cruz, F.W., Sifeddine, A., Vuille, M., Espinoza, J.C., Guyot, J.L., Khodri, M., Strikis, N., Santos, R.V., Cheng, H., Edwards, L., Carvalho, E., Santini, W., 2014. Hydroclimate variability of the northwestern Amazon Basin near the Andean foothills of Peru related to the south American Monsoon System during the last 1600 years. Clim. Past 10, 1967–1981. http://dx.doi.org/10.5194/cp-10-1967-2014.

Appleby, P.G., 2008. Three decades of dating recent sediments by fallout radionuclides: a review. The Holocene 18, 83–93. http://dx.doi.org/10.1177/0959683607085598.

Arnaud, F., Lignier, V., Revel, M., Desmet, M., Beck, C., Pourchet, M., Charlet, F., Trentesaux, A., Tribovillard, N., 2002. Flood and earthquake disturbance of 210Pb geochronology (Lake Anterne, NW Alps). Terra Nov. 14, 225–232. http://dx.doi.org/10.1046/j.1365-3121.2002.00413.x.

Astudillo, P.X., Tinoco, B.A., Graham, C.H., Latta, S.C., 2011. Assessing methods for estimating minimum population size and monitoring Andean condors (Vultur gryphus) in southern Ecuador. Ornitol. Neotrop. 22, 257–265.

Ault, T.R., Deser, C., Newman, M., Emile-Geay, J., 2013. Characterizing decadal to centennial variability in the equatorial Pacific during the last millennium. Geophys. Res. Lett. 40, 3450–3456. http://dx.doi.org/10.1002/grl.50647.

Baker, P.A., Fritz, S.C., 2015. Nature and causes of Quaternary climate variation of tropical South America. Quat. Sci. Rev. 124, 31–47. http://dx.doi.org/10.1016/j.quascirev.2015.06.011.

Bandowe, B.A.M., Fränkl, L., Grosjean, M., Tylmann, W., Mosquera, P.V., Hampel, H., Schneider, T., 2018. A 150-year record of polycyclic aromatic compound (PAC) deposition from high Andean Cajas National Park, southern Ecuador. Sci. Total Environ. 621, 1652–1663. http://dx.doi.org/10.1016/j.scitotenv.2017.10.060.

Beck, K.K., Fletcher, M.-S., Gadd, P.S., Heijnis, H., Jacobsen, G.E., 2017. An early onset of ENSO influence in the extra-tropics of the Southwest Pacific inferred from a 14, 600 year high resolution multi-proxy record from Paddy's Lake, northwest Tasmania. Quat. Sci. Rev. 157, 164–175. http://dx.doi.org/10.1016/j.quascirev.2016.12.001.

Bendix, J., Trachte, K., Palacios, E., Rollenbeck, R., Göttlicher, D., Nauss, T., Bendix, A., 2011. El Niño meets La Niña-anomalous rainfall patterns in the "traditional" El Niño region of Southern Ecuador. Erdkunde 65, 151–167. http://dx.doi.org/10.3112/erdkunde.2011.02.04.

Bird, B.W., Abbott, M.B., Vuille, M., Rodbell, D.T., Stansell, N.D., Rosenmeier, M.F., 2011. A 2,300-year-long annually resolved record of the South American summer monsoon from the Peruvian Andes. Proc. Natl. Acad. Sci. U. S. A. 108, 8583–8588. http://dx.doi.org/10.1073/pnas.1003719108.

Blaauw, M., Christen, J.A., 2011. Flexible paleoclimate age-depth models using an autoregressive gamma process. Bayesian Anal. 6, 457–474. http://dx.doi.org/10.1214/11-BA618.

Blaauw, M., Christen, J.A., 2018. rbacon: Age-Depth Modelling using Bayesian Statistics. R package version 2.3.4. https://CRAN.R-project.org/package=rbacon.

Braconnot, P., Luan, Y., Brewer, S., Zheng, W., 2012. Impact of Earth's orbit and freshwater fluxes on Holocene climate mean seasonal cycle and ENSO characteristics. Clim. Dyn. 38, 1081–1092. http://dx.doi.org/10.1007/s00382-011-1029-x.

Braganza, K., Gergis, J.L., Power, S.B., Risbey, J.S., Fowler, A.M., 2009. A multiproxy index of the El Niño-southern oscillation, a.D. 1525-1982. J. Geophys. Res. Atmos. 114, 1–17. http://dx.doi.org/10.1029/2008JD010896.

Brisset, E., Guiter, F., Miramont, C., Troussier, T., Sabatier, P., Poher, Y., Cartier, R., Arnaud, F., Malet, E., Anthony, E.J., 2017. The overlooked human influence in historic and prehistoric floods in the European Alps. Geology 45, G38498.1. http://dx.doi.org/10.1130/G38498.1.

Bustamante, M.G., Cruz, F.W., Vuille, M., Apaéstegui, J., Strikis, N., Panizo, G., Novello, F.V., Deininger, M., Sifeddine, A., Cheng, H., Moquet, J.S., Guyot, J.L., Santos, R.V., Segura, H., Edwards, R.L., 2016. Holocene changes in monsoon precipitation in the Andes of NE Peru based on δ18O speleothem records. Quat. Sci. Rev. 146, 274–287. http://dx.doi.org/10.1016/j.quascirev.2016.05.023.

Butz, C., Grosjean, M., Fischer, D., Wunderle, S., Tylmann, W., Rein, B., 2015. Hyperspectral imaging spectroscopy: a promising method for the biogeochemical analysis of lake sediments. J. Appl. Remote. Sens. 9, 1–20. http://dx.doi.org/10.1117/1.jrs.9.096031.

Cai, W., Santoso, A., Wang, G., Yeh, S.-W., An, S.-I., Cobb, K.M., Collins, M., Guilyardi, E., Jin, F.-F., Kug, J.-S., Lengaigne, M., Mcphaden, M.J., Takahashi, K., Timmermann, A., Vecchi, G., Watanabe, M., Wu, L., 2015. ENSO and greenhouse warming. Nat. Clim. Chang. 5, 849–859. http://dx.doi.org/10.1038/nclimate2743.

Chen, S., Hoffmann, S.S., Lund, D.C., Cobb, K.M., Emile-Geay, J., Adkins, J.F., 2016. A high-resolution speleothem record of western equatorial Pacific rainfall: implications for Holocene ENSO evolution. Earth Planet. Sci. Lett. 442, 61–71. http://dx.doi.org/10.1016/j.epsl.2016.02.050.

Clement, A.C., Seager, R., Cane, M.A., 2000. Suppression of El Niño during the mid-Holocene by changes in the Earth's orbit. Paleoceanography 15, 731–737. http://dx.doi.org/10.1029/1999PA000466.

Cobb, K.M., Westphal, N., Sayani, H.R., Watson, J.T., Di Lorenzo, E., Cheng, H., Edwards, R.L., Charles, C.D., 2013. Highly variable El Niño-southern oscillation throughout the Holocene. Science (80-.) 339, 67–70. http://dx.doi.org/10.1126/science.1228246.

Conroy, J.L., Overpeck, J.T., Cole, J.E., Shanahan, T.M., Steinitz-Kannan, M., 2008. Holocene changes in eastern tropical Pacific climate inferred from a Galápagos lake sediment record. Quat. Sci. Rev. 27, 1166–1180. http://dx.doi.org/10.1016/j.quascirev.2008.02.015.

Croudace, I.W., Rindby, A., Rothwell, R.G., 2006. ITRAX: description and evaluation of a new multi-function X-ray core scanner. In: Rothwell, R.G. (Ed.), New Techniques in Sediment Core Analysis. Special Publication. Geological Society, London, pp. 51–63. http://dx.doi.org/10.1144/GSL.SP.2006.267.01.04.

Donders, T.H., Wagner-Cremer, F., Visscher, H., 2008. Integration of proxy data and model scenarios for the mid-Holocene onset of modern ENSO variability. Quat. Sci. Rev. 27, 571–579. http://dx.doi.org/10.1016/j.quascirev.2007.11.010.

Emile-Geay, J., Tingley, M., 2016. Inferring climate variability from nonlinear proxies: application to palaeo-ENSO studies. Clim. Past 12, 31–50. http://dx.doi.org/10.5194/cp-12-31-2016.

Emile-Geay, J., Cobb, K.M., Mann, M.E., Wittenberg, A.T., 2013. Estimating central equatorial Pacific SST variability over the past millennium. Part II: Reconstructions and Implications. J. Clim. 26, 2329–2351. http://dx.doi.org/10.1175/JCLI-D-11-00511.1.

Garcia-Herrera, R., Diaz, H.F., Garcia, R.R., Prieto, M.R., Barriopedro, D., Moyano, R., Hernández, E., 2008. A chronology of El Niño events from primary documentary sources in northern Peru. J. Clim. 21, 1948–1962. http://dx.doi.org/10.1175/2007JCLI1830.1.

Gergis, J.L., Fowler, A.M., 2009. A History of ENSO Events Since A.D. 1525: Implications for Future Climate Change, Climatic Change. http://dx.doi.org/10.1007/s10584-008-9476-z.

Geyh, M.A., Grosjean, M., Núñez, L., Schotterer, U., 1999. Radiocarbon reservoir effect and the timing of the late-glacial/early Holocene humid phase in the Atacama Desert (Northern Chile). Quat. Res. 52, 143–153. http://dx.doi.org/10.1006/qres.1999.2060.

Gunkel, G., 2003. Limnología de un Lago tropical de Alta Montaña, en Ecuador : Características de los sedimentos y tasa de sedimentación. Rev. Biol. Trop. 51, 381–390.

Håkanson, L., Jansson, M., 2002. Principals of Lake Sedimentology. The Blackburn press, New Jersey.

Hansen, B.C.S., Rodbell, D.T., Seltzer, G.O., León, B., Young, K.R., Abbott, M., 2003. Late-glacial and Holocene vegetational history from two sites in the western Cordillera of southwestern Ecuador. Palaeogeogr. Palaeoclimatol. Palaeoecol. 194, 79–108. http://dx.doi.org/10.1016/S0031-0182(03)00272-4.

Harden, C.P., 2006. Human impacts on headwater fluvial systems in the northern and central Andes. Geomorphology 79, 249–263. http://dx.doi.org/10.1016/j.geomorph.2006.06.021.

Heiri, O., Lotter, A.F., Lemcke, G., 2001. Loss on ignition as a method for estimating organic and carbonate content in sediments: reproducibility and comparability of results. J. Paleolimnol. 25, 101–110. http://dx.doi.org/10.1023/A:1008119611481.

Horel, J.D., Cornejo-Garrido, A.G., 1986. Convection along the coast of northern Peru during 1983: spatial and temporal variation of clouds and rainfall. Mon. Weather Rev. http://dx.doi.org/10.1175/1520-0493(1986)114<2091:CATCON>2.0.CO;2.

Kalnay, E., Kanamitsu, M., Kistler, R., Collins, W., Deaven, D., Gandin, L., Iredell, M., Saha, S., White, G., Woollen, J., Zhu, Y., Chelliah, M., Ebisuzaki, W., Higgins, W., Janowiak, J., Mo, K.C., Ropelewski, C., Wang, J., Leetmaa, A., Reynolds, R., Jenne, R., Joseph, D., 1996. The NCEP/NCAR 40-year reanalysis project. Bull. Am. Meteorol. Soc. 77, 437–471. http://dx.doi.org/10.1175/1520-0477(1996)077<0437:TNYRP>2.0.CO;2.

Kanner, L.C., Burns, S.J., Cheng, H., Edwards, R.L., Vuille, M., 2013. High-resolution variability of the South American summer monsoon over the last seven millennia: insights from a speleothem record from the central Peruvian Andes. Quat. Sci. Rev. 75, 1–10. http://dx.doi.org/10.1016/j.quascirev.2013.05.008.

Kassambara, A., Mundt, F., 2017. Factoextra: Extract and Visualize the Results of Multivariate Data Analyses, R Package Version 1.0.4. https://CRAN.R-project.org/package=factoextra.

Larsson, L.A., 2003. Cybis CooRecorder - Image Coordinate Recording Program.

Mann, M.E., Zhang, Z., Hughes, M.K., Bradley, R.S., Miller, S.K., Rutherford, S., Ni, F., 2008. Proxy-based reconstructions of hemispheric and global surface temperature variations over the past two millennia. Proc. Natl. Acad. Sci. 105, 13252–13257. http://dx.doi.org/10.1073/pnas.0805721105.

Mcgregor, S., Timmermann, A., Timm, O., 2010. A unified proxy for ENSO and PDO variability since 1650. Clim. Past 6, 1–17. http://dx.doi.org/10.5194/cpd-5-2177-2009.

Morán-Tejeda, E., Bazo, J., López-Moreno, J.I., Aguilar, E., Azorín-Molina, C., Sanchez-Lorenzo, A., Martínez, R., Nieto, J.J., Mejía, R., Martín-Hernández, N., Vicente-Serrano, S.M., 2016. Climate trends and variability in Ecuador (1966-2011). Int. J. Climatol. 36, 3839–3855. http://dx.doi.org/10.1002/joc.4597.

Moy, C.M., Seltzer, G.O., Rodbell, D.T., Anderson, D.M., Moy, A.D., Seltzer, G.O., Rodbell, D.T., Andersons, D.M., 2002. Variability of El Niño/Southern Oscillation activity at millennial timescales during the Holocene epoch. Nature 420, 162–165. http://dx.doi.org/10.1038/nature01194.

PAGES 2k Consortium, 2013. Continental-scale temperature variability during the past two millennia. Nat. Geosci. 6, 339–346. http://dx.doi.org/10.1038/ngeo1797.

PAGES 2k Consortium, 2017. A global multiproxy database for temperature reconstructions of the Common Era. Sci. Data 4, 170088. http://dx.doi.org/10.1038/sdata.2017.88.

Paladines, A., Guzmán, J., Militar, Instituto Geográfico, Minas, L.M.B., Energeticos, M., 1980. Mapa geologico del Ecuador. Hoja Geolõgica de Cuenca. Escala 1, 100,000.

R Core Team, 2016. R: A Language and Environment for Statistical Computing.

Reimer, P.J., Bard, E., Bayliss, A., Beck, J.W., Blackwell, P.G., Bronk Ramsey, C., Buck, C.E., Cheng, H., Edwards, R.L., Friedrich, M., Grootes, P.M., Guilderson, T.P., Haflidason, H., Hajdas, I., Hatté, C., Heaton, T.J., Hoffmann, D.L., Hogg, A.G., Hughen, K.A., Kaiser, K.F., Kromer, B., Manning, S.W., Niu, M., Reimer, R.W., Richards, D.A., Scott, E.M., Southon, J.R., Staff, R.A., Turney, C.S.M., van der Plicht, J., 2013. IntCal13 and Marine13 radiocarbon age calibration curves 0–50,000 years cal BP. Radiocarbon 55, 1869–1887. http://dx.doi.org/10.2458/azu_js_rc.55.16947.

Rodbell, D.T., Seltzer, G.O., Anderson, D.M., Abbott, M.B., Enfield, D.B., Newman, J.H., 1999. An ~15,000-year record of El Niño-driven Alluviation in Southwestern Ecuador. Science (80-.) 283, 516–520. http://dx.doi.org/10.1126/science.283.5401.516.

Rodbell, D.T., Seltzer, G.O., Mark, B.G., Smith, J.A., Abbott, M.B., 2008. Clastic sediment flux to tropical Andean lakes: records of glaciation and soil erosion. Quat. Sci. Rev. 27, 1612–1626. http://dx.doi.org/10.1016/j.quascirev.2008.06.004.

Salazar, G., Zhang, Y.L., Agrios, K., Szidat, S., 2015. Development of a method for fast and automatic radiocarbon measurement of aerosol samples by online coupling of an elemental analyzer with a MICADAS AMS. Nucl. Instruments Methods Phys. Res. Sect. B Beam Interact. Mater. Atoms 361, 163–167. http://dx.doi.org/10.1016/j.nimb.2015.03.051.

Schillereff, D.N., 2015. A review of in situ measurement techniques for investigating suspended sediment dynamics in lakes. Geomorphol. Tech. 3, 1–12.

Schillereff, D.N., Chiverrell, R.C., MacDonald, N., Hooke, J.M., 2014. Flood stratigraphies in lake sediments: a review. Earth Sci. Rev. 135, 17–37. http://dx.doi.org/10.1016/j.earscirev.2014.03.011.

Schnurrenberger, D., Russell, J., Kelts, K., 2003. Classification of lacustrine sediments based on sedimentary components. J. Paleolimnol. 29, 141–154. http://dx.doi.org/10.1023/A:1023270324800.

Schultheiss, P.J., Weaver, P.P.E., 1992. Multi-Sensor core logging for Science and Industry. In: Dorman, C.E. (Ed.), OCEANS 92 Proceedings: Mastering the oceans through technology. IEEE, Newport, pp. 608–613. http://dx.doi.org/10.1109/OCEANS.1992.607652.

Stenseth, N.C., Mysterud, A., Ottersen, G., Hurrell, J.W., Chan, K.S., Lima, M., 2002. Ecological effects of climate fluctuations. Science (80-.) 297, 1292–1296. http://dx.doi.org/10.1126/science.1071281.

Sulca, J., Takahashi, K., Espinoza, J.C., Vuille, M., Lavado-Casimiro, W., 2018. Impacts of different ENSO flavors and tropical Pacific convection variability (ITCZ, SPCZ) on austral summer rainfall in South America, with a focus on Peru. Int. J. Climatol. 38, 420–435. http://dx.doi.org/10.1002/joc.5185.

Szidat, S., Salazar, G.A., Vogel, E., Battaglia, M., Wacker, L., Synal, H.-A., Türler, A., 2014. 14C analysis and sample preparation at the new bern laboratory for the analysis of radiocarbon with AMS (LARA). Radiocarbon 56, 561–566. http://dx.doi.org/10.2458/56.17457.

Tylmann, W., Bonk, A., Goslar, T., Wulf, S., Grosjean, M., 2016. Calibrating 210Pb dating results with varve chronology and independent chronostratigraphic markers: problems and implications. Quat. Geochronol. 32, 1–10. http://dx.doi.org/10.1016/j.quageo.2015.11.004.

Vicente-Serrano, S.M., Aguilar, E., Martínez, R., Martín-Hernández, N., Azorin-Molina, C., Sanchez-Lorenzo, A., El Kenawy, A., Tomás-Burguera, M., Moran-Tejeda, E., López-Moreno, J.I., Revuelto, J., Beguería, S., Nieto, J.J., Drumond, A., Gimeno, L., Nieto, R., 2017. The complex influence of ENSO on droughts in Ecuador. Clim. Dyn. 48, 405–427. http://dx.doi.org/10.1007/s00382-016-3082-y.

von Gunten, L., Grosjean, M., Beer, J., Grob, P., Morales, A., Urrutia, R., 2009. Age modeling of young non-varved lake sediments: methods and limits. Examples from two lakes in Central Chile. J. Paleolimnol. 42, 401–412. http://dx.doi.org/10.1007/s10933-008-9284-5.

Vuille, M., Bradley, R.S., Keimig, F., 2000. Climate variability in the Andes of Ecuador and its relation to tropical Pacific and Atlantic Sea surface temperature anomalies. J. Clim. 13, 2520–2535. http://dx.doi.org/10.1175/1520-0442(2000)013<2520:CVITAO>2.0.CO;2.

Wang, C., Deser, C., Yu, J.-Y., Dinezio, P., Clement, A., 2017. El Niño and Southern Oscillation (ENSO): a review. In: Glynn, P.W., Manzello, D.P., Enochs, I.C. (Eds.), Coral Reefs of the Eastern Pacific: Persistence and Loss in a Dynamic Environment. Springer Science, Dordrecht, pp. 85–106. http://dx.doi.org/10.1007/978-94-017-7499-4_4.

Ward, P.J., Beets, W., Bouwer, L.M., Aerts, J.C.J.H., Renssen, H., 2010. Sensitivity of river discharge to ENSO. Geophys. Res. Lett. 37, 1–6. http://dx.doi.org/10.1029/2010GL043215.

Wilhelm, B., Vogel, H., Crouzet, C., Etienne, D., Anselmetti, F.S., 2016. Frequency and intensity of palaeofloods at the interface of Atlantic and Mediterranean climate domains. Clim. Past 12, 299–316. http://dx.doi.org/10.5194/cp-12-299-2016.

Wille, M., Hooghiemstra, H., Hofstede, R., Fehse, J., Sevink, J., 2002. Upper forest line reconstruction in a deforested area in northern Ecuador based on pollen and vegetation analysis. J. Trop. Ecol. 18, 409–440. http://dx.doi.org/10.1017/S0266467402002286.

Wilson, R., Cook, E., D'Arrigo, R., Riedwyl, N., Evans, M.N., Tudhope, A., Allan, R., 2010. Reconstructing ENSO: the influence of method, proxy data, climate forcing and teleconnections. J. Quat. Sci. 25, 62–78. http://dx.doi.org/10.1002/jqs.1297.

Yan, H., Sun, L., Wang, Y., Huang, W., Qiu, S., Yang, C., 2011. A record of the southern oscillation index for the past 2,000 years from precipitation proxies. Nat. Geosci. 4, 611–614. http://dx.doi.org/10.1038/ngeo1231.

Zhang, Z., Leduc, G., Sachs, J.P., 2014. El Niño evolution during the Holocene revealed by a biomarker rain gauge in the Galápagos Islands. Earth Planet. Sci. Lett. 404, 420–434. http://dx.doi.org/10.1016/j.epsl.2014.07.013.